Supporting Information for

Role of synergic interaction in transition state formation of aldol reaction on metal oxide catalyst: A DFT investigation

Wei An[a,*]

[a]College of Chemistry and Chemical Engineering, Shanghai University Of Engineering Science, Shanghai 201620, China. [*]E-mail: weian@sues.edu.cn

S1 Computational details

S1.1 Methods

All calculations were performed by using density-functional theory (DFT) as implemented in Vienna ab-initio simulation package (VASP).[1-2] The interaction between ions and electrons is described using the projector augmented wave (PAW) method.[3-4] The Kohn–Sham orbitals are expanded in a plane-wave basis set with a kinetic energy cutoff of 400 eV. The spin-polarized GGA-PW91 exchange-correlation functional[5] was used with [Zr]-$4s^2 4p^6 5s^2 4d^2$, [Ce]-$5s^2 5p^6 6s^2 4f^1 5d^1$, [O]-$2s^2 2p^4$, [C]-$2s^2 2p^2$, and [H]-1s treated as valence electrons. The conjugate gradient algorithm was used in optimization and the convergence threshold was set to be 10^{-3} eV in total energy and 0.02 eV/Å in Hellmann-Feynman force on each atom. The calculated equilibrium lattice constant was obtained using the tetrahedron method with Blöchl corrections[6] and a Monkhorst–Pack[5] grid of 10×10×10 *k*-points, with the convergence criteria of 10^{-6} eV in total energy and 10^{-5} eV /Å in force. For surface calculations, the Brillouin zone integration is performed using Γ point only for a *p*(4×4) lateral supercell. Our test calculations show that increasing k-points has only negligible effect on the results (±0.1kcal/mol difference in binding energy by using 3×3×1 *k*-points). All reported energies were extrapolated to k_BT = 0 eV. The climbing-image nudged elastic band (CI-NEB) method[7-8] was used to locate the TS structure along the minimum-energy pathway (MEP) for aldol reaction of propanal and interconversion of propanal rotamers. Spring constant of 5.0 eV/Å^2 and ten images were used.

The binding energy (BE) is defined as $BE = E_{(ads/slab)} - E_{slab} - E_{(ads)}$, where $E_{(ads/slab)}$, E_{slab}, and $E_{(ads)}$ are the total energy of ads/slab, clean surface, and gas-phase adsorbate molecule.

It's been known that LDA+U and GGA+U methods[9-11] are commonly employed for ceria with strongly localized Ce-4f electrons, particularly for defective ceria,[12] in order to correctly address the electronic structure of ceria. In DFT+U approach, on-site electron-electron Coulomb repulsion (the empirical Hubbard U term) and exchange (parameter J) interactions are introduced to capture the correct electronic features of strongly-correlated Ce-4f electrons and their localization. We also examined such effect in our calculations. By employing the GGA+U approach by Dudarev *et al.* [13] with U = 7.0 eV and J = 0.7 eV,[11] we obtained a slightly increased BE for adsorbates on O-terminated CeO_2 (111) surface. Nevertheless, the GGA+U method does not change the overall trend of the energetics and thus the conclusions by employing GGA-DFT method in this work. The same approach has been used in previous DFT studies.[14-15] It's worthy to note that DFT+U method is indeed critical to reduced CeO_2 (111) surface. For example, for adsorption of propanal at O-vacancy site of CeO_2 (111) surface, the calculated BE is -34.2 kcal/mol (DFT+U) vs -19.6 kcal/mol (GGA-DFT), which is consistent with previous findings.[16-17]

S1.2 Slab model

The under-coordination of the surface and the ionic nature of both ZrO_2 and CeO_2 render surface metal Zr and Ce sites with Lewis acidity and O sites with Lewis basicity. It's known that zirconia undergoes phase transition from monoclinic (<1,170 °C) to tetragonal (1,170–2,370 °C) and eventually to cubic structures (>2,370 °C). At the temperature relevant to aldol condensation (<1,170 °C), monoclinic ZrO_2 (Zr_{CN} = 7, O_{CN} = 3 and 4) is the most stable phase.[18] Since our study is aimed to explore the effects of acid-base pair strength on the aldol reaction, we therefore adopted cubic structure for both ZrO_2 and CeO_2 in our calculations (Figure S1 and S2), in order to isolate geometrical effect and therefore for a more direct comparison. The O-terminated surfaces are most abundant from nanoparticle catalysts.[19-20] Both O-terminated CeO_2(111) surface[10, 14-15, 21-22] and O-terminated ZrO_2(111) surface[23-24] were employed in previous DFT studies. The ZrO_2(111) surface was modeled by a slab in a *p*(4×4) lateral supercell (14.38 Å × 14.38 Å × 19.54 Å), which contains three (O-Zr-O) repeating units, a total of nine layers (96 O atoms and 48 Zr atoms), and is sufficiently large to accommodates two propanal molecules with

negligible lateral interactions with their images. The two successive slabs were separated by a 13 Å vacuum region to ensure negligible normal interactions between adsorbates and slab image. Dipole moment normal to the surface is eliminated with O-terminated surface at both top and bottom layers. In calculations, the bottom six layers (i.e., two ZrO_2 trilayers) were fixed at their equilibrium bulk phase positions with calculated lattice constant of 5.085 Å (5.070Å by experiment), while the top three layers (i.e., one ZrO_2 trilayers) and all adsorbates were allowed to relax without geometrical constraints. The top layer features $(ZrO)_3$ or $(CeO)_3$ six-member rings [Figure S1 and S2].

The O-terminated CeO_2 (111) surface was modeled in the same fashion as the ZrO_2(111) surface. The *p*(4×4) supercell has a dimension of 15.32 Å × 15.32 Å × 20.17 Å. The calculated lattice constant is 5.418 Å (5.411Å by experiment), which is similar to 5.419 Å obtained in previous work using GGA-PW91 functional.[25]

We also verified the validity of methods and models used in this work by calculating surface energy of O-terminated CeO_2(111) and ZrO_2(111) surface. The surface energy is expressed as:[26]

$$\sigma = \frac{1}{2A}(E_{slab} - \frac{Ns}{Nb}E_{bulk}) \qquad (1)$$

where σ, A, E_{slab}, and E_{bulk} are the surface energy, surface area, total energy of the slab (containing *Ns* atoms) and the bulk (containing *Nb* atoms), respectively. Lower σ value indicates a more stable surface and less surface reactivity. We obtained σ value of 0.54 and 0.70 J/m^2 for relaxed O-terminated CeO_2 (111) and ZrO_2(111) surface, respectively, which are lower than those from previous work, but exhibit the same trend.[15, 21]

S2 Projected-density of states (DOS)

Figure S5 shows the projected-DOS of labeled H, C, O atoms of TS1, MS1, TS2, MS2 in Figure 2. In Figure S5(a), one can see that the "residual" 1s-states of α-H in TS1 (blue line), i.e., $H^{\delta+}$ instead of a proton H^{1+}, is significantly broadened by 2p-states of both α-C of rotamer B and O of ZrO_2 on the surface and have a large overlap below Fermi level, an indication of direct electronic interactions among C•••H•••O in TS1. In comparison, the strongly localized 1s-states of the dissociated α-H can be found at -7.8eV with complete overlap with 2p-states of surface O [Figure S5(b)], indicating the formation of strong O-H bond in MS1. In Figure S5(c), the 1s-states of the same H in TS2 is mainly localized at -7.5eV below Fermi level and has large

overlaps with 2p-states of both surface O of ZrO_2 (yellow line) and carbonyl O of rotamer A (red line), suggesting a direct electronic interactions among O•••H•••O in TS2. The peaks resemble those of MS2 with only slight shift [Figure S5(d)]. The "residual" 1s-states are populated 22% less in magnitude than those of TS1, an outcome of high electron-pulling capacity from two O in TS2.

Table S1. Characteristic bond lengths of propanal (A) and (B) along MEP for aldol reaction on (a) ZrO_2(111) surface and (b) CeO_2(111) surface, as shown in Figure 1 and Figure S2. Values in bold correspond to bond break and formation.

(a)

Bond length (Å)	IS	TS1	MS1	MS2	TS2	MS2	FS
Zr-O(B)	2.317	2.135	1.991	2.042	2.131	2.307	4.981
O⋯H_α(B)	2.185	**1.496**	0.978	0.990	**1.263**	1.880	-
C_α(B)-H_α(B)	1.107	**1.292**	2.703	-	-	-	-
C(B)-O(B)	1.236	1.272	1.344	1.348	1.258	1.233	1.217
C(B)-C_α(B)	1.486	1.404	1.345	1.345	1.425	1.490	1.515
Zr-O(A)	-	-	-	2.389	-	-	-
C(A)-O(A)	-	-	-	1.225	1.336	1.420	1.440
C(A)-C_α(A)	-	-	-	1.494	1.540	1.540	1.534
H_α(B)-O(A)	-	-	-	2.675	**1.190**	0.994	0.974
C_α(B)-C(A)	-	-	-	3.953	**1.865**	1.570	1.537

(b)

Bond length (Å)	IS	TS1	MS1	MS2	TS2	MS2	FS
Ce-O(B)	2.631	2.425	2.213	2.229	2.499	2.611	4.500
O⋯H_α(B)	2.586	**1.367**	0.979	0.977	**1.203**	1.769	-
C_α(B)-H_α(B)	1.107	**1.397**	2.772	-	-	-	-
C(B)-O(B)	1.226	1.261	1.322	1.318	1.232	1.224	1.217
C(B)-C_α(B)	1.498	1.425	1.359	1.359	1.474	1.498	1.515
Ce-O(A)	-	-	-	2.663	-	-	-
C(A)-O(A)	-	-	-	1.225	1.384	1.424	1.442
C(A)-C_α(A)	-	-	-	1.494	1.555	1.539	1.534
H_α(B)-O(A)	-	-	-	2.442	**1.252**	1.000	0.974
C_α(B)-C(A)	-	-	-	3.978	**1.675**	1.562	1.534

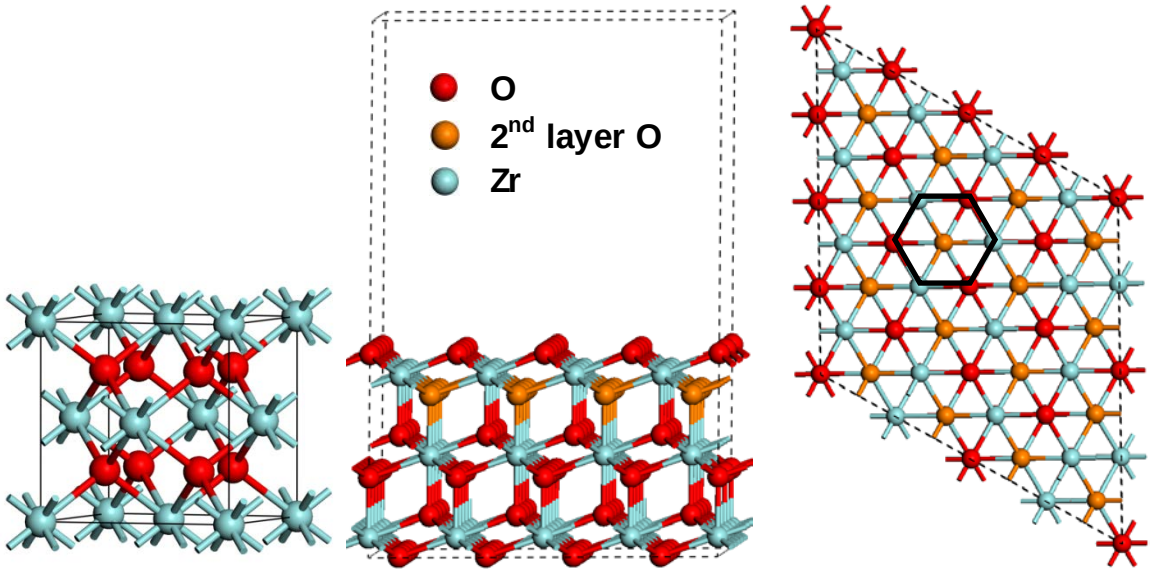

Figure S1. (a) Optimized structure of (a) ZrO_2 cubic unit cell; (b) Side view and (c) Top view of O-terminated ZrO_2(111) surface in a supercell. Top layer features $(ZrO)_3$ six-member ring (black hexagon) with second-layer O centered underneath. Bulk: Zr_{CN} = 8, O_{CN} = 4; Surface: Zr_{CN} = 7, O_{CN} = 3. CN: coordination number.

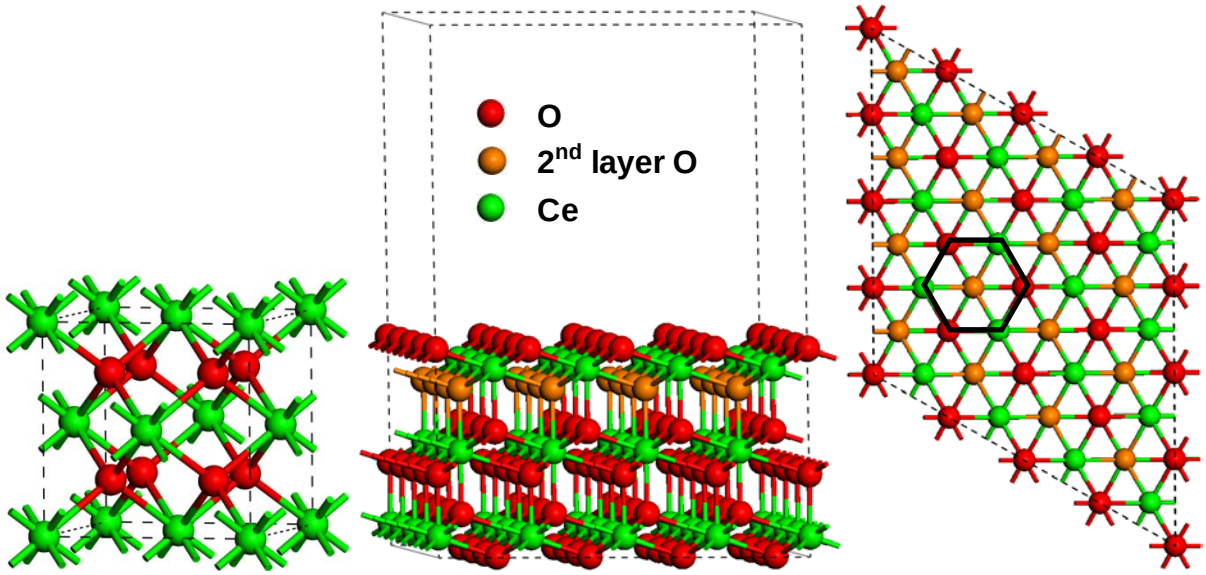

Figure S2. (a) Optimized structure of (a) CeO_2 cubic unit cell; (b) Side view and (c) Top view of O-terminated CeO_2(111) surface in a supercell. Top layer features $(CeO)_3$ six-member ring (black hexagon) with second-layer O centered underneath. Bulk: Ce_{CN} = 8, O_{CN} = 4; Surface: Ce_{CN} = 7, O_{CN} = 3.

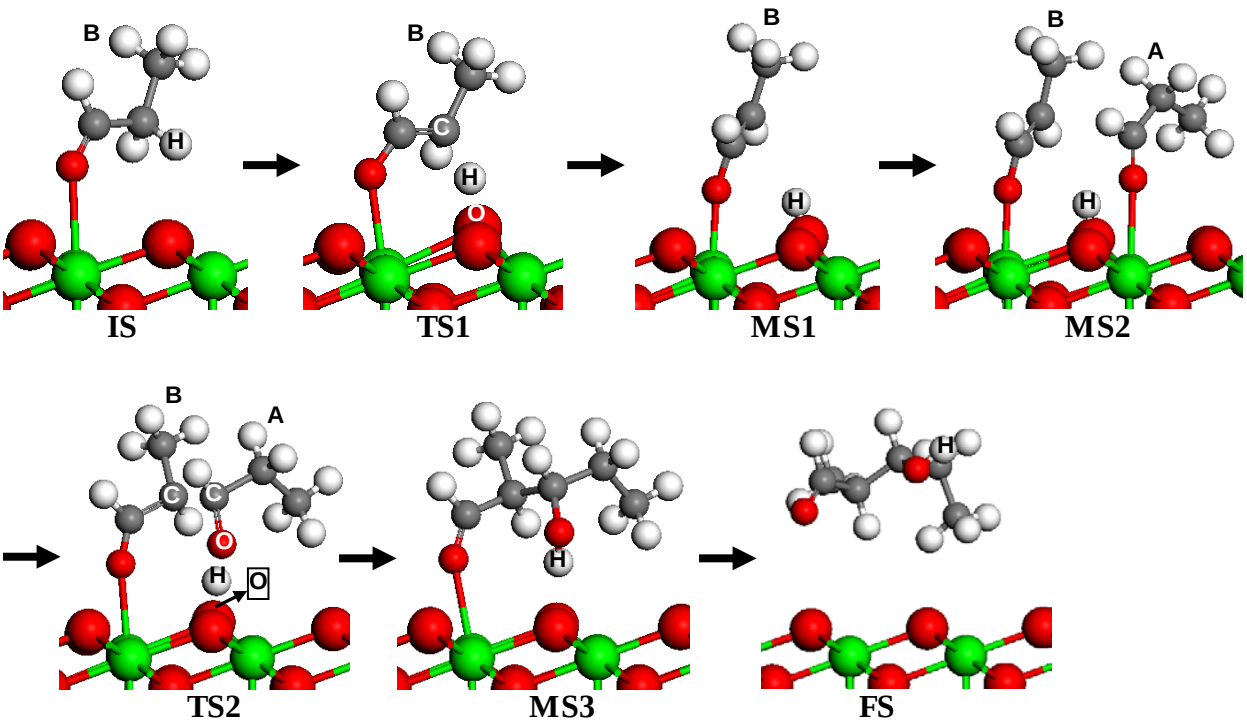

Figure S3. Evolution of geometrical structures along MEP for aldol reaction of propanal on O-terminated CeO2(111) surface during one catalytic turnover. Imaginary frequencies: i1373.7cm^{-1} (TS1), i729.4cm^{-1} (TS2)

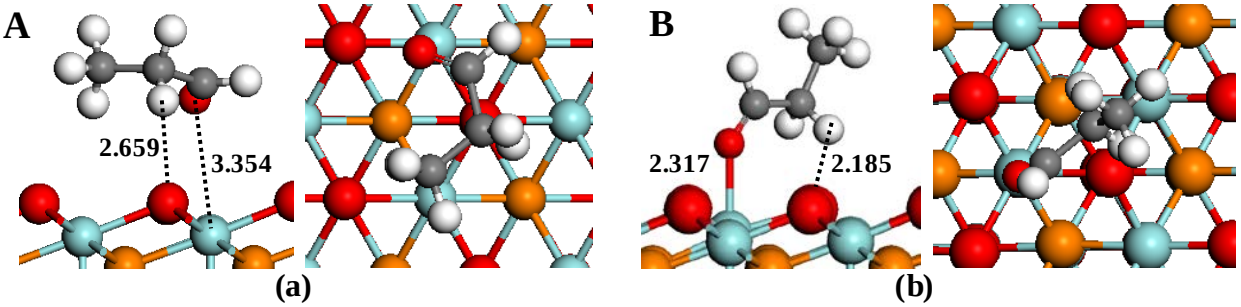

Figure S4. Comparison of adsorption of two rotamer A and B on O-terminated ZrO_2(111) surface. (a) A, BE = -1.8kcal/mol; (b) B, BE = -8.7 kcal/mol.

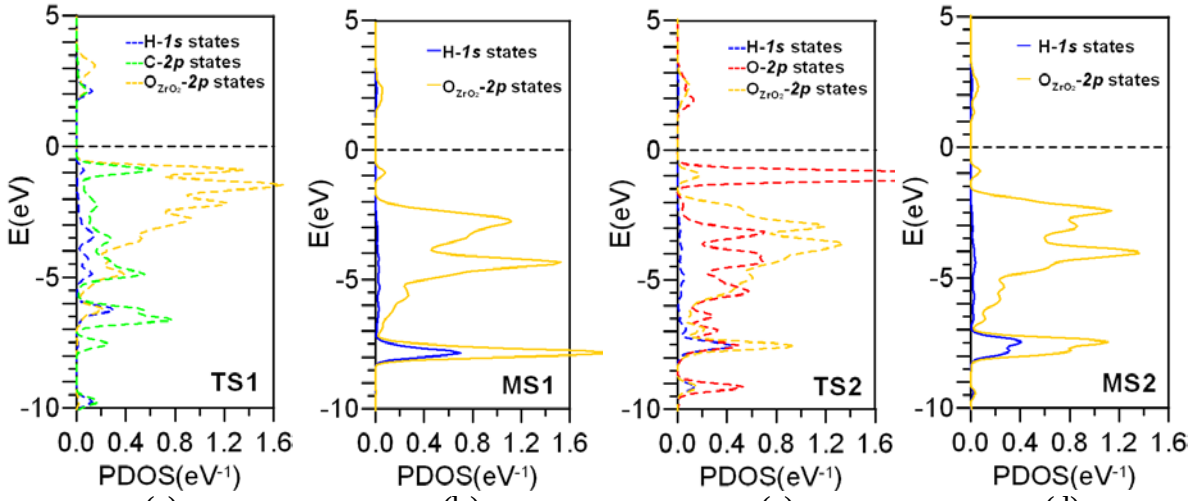

Figure S5. Calculated PDOS for labeled H, C, and O atoms in Figure 2. (a) TS1, (b) MS1, (c) TS2, and (d) MS2. Zero-line represents Fermi level.

References

1 G. Kresse and J. Hafner, Abinitio Molecular-Dynamics for Liquid-Metals, *Phys. Rev. B* 1993, **47**, 558.

2 G. Kresse and J. Furthmuller, Efficient iterative schemes for ab initio total-energy calculations using a plane-wave basis set, *Phys. Rev. B* 1996, **54**, 11169.

3 P. E. Blochl, Projector Augmented-Wave Method, *Phys. Rev. B* 1994, **50**, 17953.

4 G. Kresse and D. Joubert, From ultrasoft pseudopotentials to the projector augmented-wave method, *Phys. Rev. B* 1999, **59**, 1758.

5 J. P. Perdew, J. A. Chevary, S. H. Vosko, K. A. Jackson, M. R. Pederson, D. J. Singh and C. Fiolhais, Atoms, Molecules, Solids, and Surfaces - Applications of the Generalized Gradient Approximation for Exchange and Correlation, *Phys. Rev. B* 1992, **46**, 6671.

6 P. E. Blochl, O. Jepsen and O. K. Andersen, Improved Tetrahedron Method for Brillouin-Zone Integrations, *Phys. Rev. B* 1994, **49**, 16223.

7 G. Henkelman, B. P. Uberuaga and H. Jonsson, A climbing image nudged elastic band method for finding saddle points and minimum energy paths, *J. Chem. Phys.* 2000, **113**, 9901.

8 G. Mills, H. Jonsson and G. K. Schenter, Reversible Work Transition-State Theory - Application to Dissociative Adsorption of Hydrogen, *Surf. Sci.* 1995, **324**, 305.

9 D. A. Andersson, S. I. Simak, B. Johansson, I. A. Abrikosov and N. V. Skorodumova, Modeling of CeO2, Ce2O3, and CeO2-x in the LDA plus U formalism, *Phys. Rev. B* 2007, **75**, 035109.

10 M. Nolan, S. Grigoleit, D. C. Sayle, S. C. Parker and G. W. Watson, Density functional theory studies of the structure and electronic structure of pure and defective low index surfaces of ceria, *Surf. Sci.* 2005, **576**, 217.

11 Y. Jiang, J. B. Adams and M. van Schilfgaarde, Density-functional calculation of CeO2 surfaces and prediction of effects of oxygen partial pressure and temperature on stabilities, *J. Chem. Phys.* 2005, **123**, 064701.

12 H. F. Wang, H. Y. Li, X. Q. Gong, Y. L. Guo, G. Z. Lu and P. Hu, Oxygen vacancy formation in CeO2 and Ce1-xZrxO2 solid solutions: electron localization, electrostatic potential and structural relaxation, *Phys Chem Chem Phys* 2012, **14**, 16521.
13 S. L. Dudarev, G. A. Botton, S. Y. Savrasov, C. J. Humphreys and A. P. Sutton, Electron-energy-loss spectra and the structural stability of nickel oxide: An LSDA+U study, *Phys. Rev. B* 1998, **57**, 1505.
14 E. Skulason, G. S. Karlberg, J. Rossmeisl, T. Bligaard, J. Greeley, H. Jonsson and J. K. Norskov, Density functional theory calculations for the hydrogen evolution reaction in an electrochemical double layer on the Pt(111) electrode, *Phys Chem Chem Phys* 2007, **9**, 3241.
15 Z. X. Yang, T. K. Woo, M. Baudin and K. Hermansson, Atomic and electronic structure of unreduced and reduced CeO2 surfaces: A first-principles study, *J. Chem. Phys.* 2004, **120**, 7741.
16 M. Nolan, S. C. Parker and G. W. Watson, Reduction of NO2 on ceria surfaces, *J. Phys. Chem. B* 2006, **110**, 2256.
17 M. Nolan, S. C. Parker and G. W. Watson, CeO2 catalysed conversion of CO, NO2 and NO from first principles energetics, *Phys. Chem. Chem. Phys.* 2006, **8**, 216.
18 A. Christensen and E. A. Carter, First-principles study of the surfaces of zirconia, *Phys. Rev. B* 1998, **58**, 8050.
19 M. A. Henderson, C. L. Perkins, M. H. Engelhard, S. Thevuthasan and C. H. F. Peden, Redox properties of water on the oxidized and reduced surfaces of CeO2(111), *Surf. Sci.* 2003, **526**, 1.
20 X. D. Feng, D. C. Sayle, Z. L. Wang, M. S. Paras, B. Santora, A. C. Sutorik, T. X. T. Sayle, Y. Yang, Y. Ding, X. D. Wang and Y. S. Her, Converting ceria polyhedral nanoparticles into single-crystal nanospheres, *Science* 2006, **312**, 1504.
21 M. Fronzi, A. Soon, B. Delley, E. Traversa and C. Stampfl, Stability and morphology of cerium oxide surfaces in an oxidizing environment: A first-principles investigation, *J. Chem. Phys.* 2009, **131**, 104701.
22 S. Fabris, G. Vicario, G. Balducci, S. de Gironcoli and S. Baroni, Electronic and atomistic structures of clean and reduced ceria surfaces, *J. Phys. Chem. B* 2005, **109**, 22860.
23 R. Grau-Crespo, N. C. Hernandez, J. F. Sanz and N. H. de Leeuw, Theoretical investigation of the deposition of Cu, Ag, and Au atoms on the ZrO2(111) surface, *J. Phys. Chem. C* 2007, **111**, 10448.
24 H. J. Li and J. J. Ho, Mechanism of CH2 Steam Reforming on a Rh/ZrO2(111) Surface: A Computational Study, *J. Phys. Chem. C* 2009, **113**, 20139.
25 H. T. Chen, Y. M. Choi, M. L. Liu and M. C. Lin, A theoretical study of surface reduction mechanisms of CeO2 (111) and (110) by H-2, *Chemphyschem* 2007, **8**, 849.
26 V. Fiorentini and M. Methfessel, Extracting convergent surface energies from slab calculations, *J. Phys. Condens. Matter* 1996, **8**, 6525.